Bedload and Concentration Effects on Turbulent Suspension Properties in Heavy Particle Sheet Flows

Hélder Guta, David Hurther, Julien Chauchat

Bedload and Concentration Effects on Turbulent Suspension Properties in Heavy Particle Sheet Flows

Hélder Guta[1]; David Hurther[2]; and Julien Chauchat[3]

Abstract: A new set of open-channel flow experiments and turbulence resolved data are presented in heavy particle sheet flows (Shields number $0.35 \leq \theta \leq 0.85$) for which the proportions of bedload and suspended load are both important (ratio of settling velocity and friction velocity in the range $0.8 \leq w_s/u_* \leq 1.3$). The effects of sediments and particularly the bedload on the turbulent suspension have been addressed by gradually increasing the concentration from clear water to capacity conditions. Distinction between the bedload and the suspension layer is discussed on the basis of the linearity of turbulent mixing length profiles. It is shown that the bedload layer has important impact on the vertical structure of the particle-laden flow. An upward shift of the logarithmic velocity layer is seen to be accompanied by a strong reduction of turbulent momentum mixing. The modification of the mixing length affects the theoretical formulation of both velocity and concentration profiles in the suspension layer. A modified analytical solution is derived for the suspended sediment concentration profile taking into account the presence of the bedload layer for improved predictions compared with the classical Rouse equation. Based on the present experiments, as well as literature data, an alternative parametrization for the β-factor (ratio of sediment and momentum diffusivities) is proposed over an extended range of suspension number, $0 < w_s/u_* < 1.5$. **DOI: 10.1061/(ASCE)HY.1943-7900.0001988.**

Introduction

Modeling intense sediment transport caused by high bed-shear stress is of primary engineering and environmental interest. Such conditions are encountered typically during river floods and coastal storms, which have a major impact on short- to long-term river morphology and coastal shoreline evolutions. This is especially true in the context of abrupt climate change and sustainable adaptation strategy.

When the dimensionless bed-shear stress defined as the $\theta = \rho_f u_*^2/(\rho_p - \rho_f)gd_p$ (where ρ_f and ρ_p are the fluid and particle densities, respectively; u_* is the friction velocity; d_p is the particle diameter; and g is the acceleration of gravity) exceeds a critical value of approximately 0.4 (Rickenmann 1991; García 2008), energetic bedload transport occurs in a layer with thickness of several particle diameters d_p (Wilson 1987). In such conditions, bedforms are washed out and the sediment bed becomes plane. This is known as sheet-flow or upper stage plane bed regime (Sumer et al. 1996). In this regime, the hydraulic resistance and the relative bed roughness scale with the thickness of the bedload layer rather than the skin roughness elements themselves (Wilson 1989; Sumer et al. 1996; Ribberink et al. 2008). Whether a sheet flow carries a higher fraction of the transported sediment load as a turbulent suspension load or as bedload depends on the ratio between the particle's settling velocity w_s and the bed friction velocity u_*. This ratio is named the suspension number $S = w_s/u_*$ in Sumer et al. (1996), who observed that the transition from the suspension mode to the no-suspension mode occurs around $S \approx 0.8$–1. The no-suspension sheet-flow regime is sometimes called heavy particle or massive particle transport (Wilson 1989; Sumer et al. 1996; Ribberink et al. 2008) because particles are too heavy to be permanently entrained into the water column by turbulent flow structures generated in the bottom shear boundary layer. By extending the range of suspension number values originally studied by Wilson (1989), Sumer et al. (1996) noticed that some properties of sheet flows depend on whether it occurs in suspension ($S < 0.8$) or no-suspension mode ($S > 1$). Recently, Finn and Li (2016) represented all possible types of sediment-turbulence regimes in the well-known Shields diagram. Their results suggest that the domain covering the range $0.8 < S < 1.3$ with $\theta > 0.8$, corresponds to sheet flows of medium to large sand or gravel particles. This type of intense sediment-laden flows represents a frequently established flow case during river floods and coastal storms and therefore merits to be studied from a physical process-oriented point of view in order to improve our numerical prediction ability of sediment transport and bed morphology evolution.

In such sheet-flow conditions, the conventional bedload formulas do not predict reliable sediment transport rates because complex turbulent particle mixing, turbulence-particle interactions, as well as particle-particle interaction processes all play important different roles across the bottom boundary layer (Revil-Baudard et al. 2015, 2016). The modifications of the turbulent boundary layer in intense sediment-laden flow conditions implies greater efforts in the parametrization of classical laws such as the log-law and Rouse profiles for velocity and concentration distribution, respectively. For example, van Rijn (1984) concluded that more research effort was necessary to provide new parametrized velocity profile formulations valid for heavy sediment-laden flows. He stressed that the standard

[1]Ph.D. Student, Laboratoire des Écoulements Géophysiques et Industriels/Centre National de Recherches Scientifiques/Université Grenoble Alpes, Dept. of Earth, Planet, and Environment Sciences, Grenoble Alpes Univ., Domaine Universitaire, BP 53, 38041 Grenoble CEDEX 9, France (corresponding author). Email: helder.guta@univ-grenoble-alpes.fr

[2]Research Director, Laboratoire des Écoulements Géophysiques et Industriels/Centre National de Recherches Scientifiques/Université Grenoble Alpes, Dept. of Earth, Planet, and Environment Sciences, Grenoble Alpes Univ., Domaine Universitaire, BP 53, 38041 Grenoble CEDEX 9, France. Email: david.hurther@univ-grenoble-alpes.fr

[3]Assistant Professor, Laboratoire des Écoulements Géophysiques et Industriels/GRENOBLE-INP/Université Grenoble Alpes, Dept. of Earth, Planet, and Environment Sciences, Grenoble Alpes Univ., Domaine Universitaire, BP 53, 38041 Grenoble CEDEX 9, France. Email: julien.chauchat@univ-grenoble-alpes.fr

Note. This manuscript was submitted on June 16, 2021; approved on February 14, 2022; published online on May 9, 2022. Discussion period open until October 9, 2022; separate discussions must be submitted for individual papers. This paper is part of the ***Journal of Hydraulic Engineering***, © ASCE, ISSN 0733-9429.

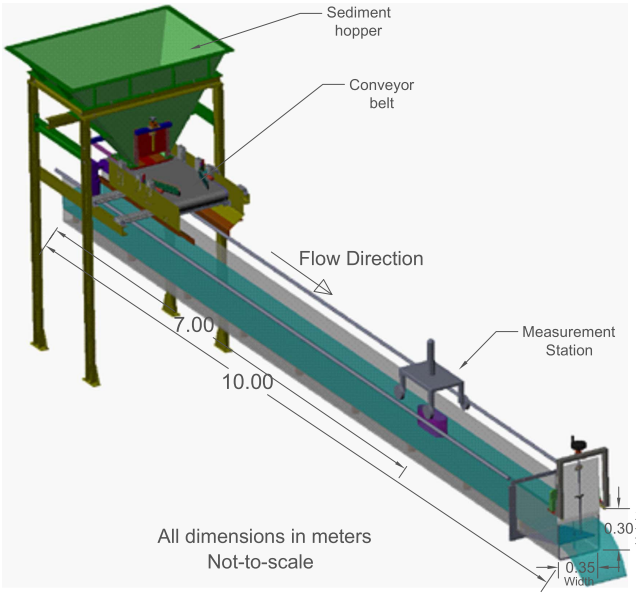

Fig. 1. Sketch of experimental set up.

logarithmic velocity distribution was not able to predict the vertical velocity structure accurately enough to derive reliable sediment transport rates. Similar conclusions were drawn concerning the concentration distribution.

In the present study, we focus on high bed-shear stress regimes ($\theta \geq 0.4$) with suspension numbers values of the order of $S \approx$ 0.8–1.3. These challenging flow conditions have been rarely investigated in the literature despite their frequent occurrence in natural sediment-laden flows. Using high-resolution measurements, we investigated the vertical flow structure with particular attention given to potential bedload layer effects on the mean velocity and concentration profiles in the suspension layer.

Experimental Setup and Flow Conditions

The experiments were carried out in the LEGI/Ecole Normale Supérieur de l'Energie, l'Eau et l'Environnent (ENSE3) tilting flume, 10-m long, and 0.35-m wide (Fig. 1). The particles used in the present experiments were low-density plastic particles (poly-methyl methacrylate $\rho_p = 1{,}192$ kg/m^3) irregularly shaped, with a uniform size distribution having a median diameter $d_p =$ 3 mm ($d_{10} = 2$ mm and $d_{90} = 4.8$ mm). The measured settling velocity of the particles in still water is $w_s = 56 \pm 9$ cm/s, hence, the associated range of variability is about 17% (Revil-Baudard et al. 2015). Reduction of w_s due to potential concentration effects was evaluated with Richardson-Zaki type equation. The maximum estimated decrease (5%) remained within the accuracy range of the measured w_s, hence, the still water value was applied for all solid load conditions. The fixed bed was covered by glued particles with the same properties as the ones transported by the flow. To enhance the full development of the turbulent boundary layer, a honeycomb at the flume inlet, followed by a macroroughness bed surface extended over about 50 cm, were used. The experiments covered three flow conditions obtained by imposing a flow discharge Q and a bed slope S_0, as given in Table 1. The experimental runs all had a duration of 300 s to guarantee low statistical bias of the measured high-order statistical moments. The measurements were carried out in sequences that started with a clear-water (CW) run, followed by one, two, or three sediment-laden (SL) runs. This ensured that all runs were performed in the exact same flow configuration and setup, with only the addition of sediments (see Supplemental Materials for a full list of experimental sequences). The position of the fixed rigid bed (the zero vertical level) for all sediment-laden runs is identified based on the corresponding clear-water runs, because it is easier to detect it without a moving sediment layer covering the bed. Note that this is justified in the present conditions, given that there is no permanent deposition (no particles at rest over the fixed rigid bed), even in capacity conditions. The injected solid load in saturation was defined experimentally as the beginning of sediment deposition at the bed (from visual observation). It corresponds to the condition for which significant increase in the injected solid load would lead to continuous deposition of sediments on the bed. Since the convergence to full transport capacity is relatively subjective, the degree of saturation is to some extent uncertain (Lyn 1986). Hence, the saturated cases correspond to conditions around full-capacity regime. The injected solid load Q_s^{inj} for the two regimes below capacity was fixed based on the desired mean volumetric concentration, given as the ratio between the injected solid load and the flow discharge, such that $Q_s^{inj} = C^{inj} \times Q$. The defined mean volumetric concentrations are approximately $C^{inj} \approx 6 \times 10^{-4}$ and 2×10^{-3}, for the lower (LOW) and the

Table 1. Flow conditions for the three hydraulic conditions, each with four solid transport regimes from clear water to full capacity

u_* (m/s)	Θ	S	Q (m^3/s)	S_0	U (m/s)	H_f (m)	Re	Fr	Re_*	q_s (m^2/s)	$\bar{C}$	Runs
0.044	0.35	1.3	0.032	0.0023	0.61	0.15	1.9×10^5	0.51	131	0.0	0.0	8 CW runs
										6.7×10^{-5}	1.2×10^{-3}	P3S03D4_LOW[a], P3S03D5_LOW, P3S03D6_LOW
										1.4×10^{-4}	2.6×10^{-3}	P3S03D4_MED[a], P3S03D7_MED, P3S03D8_MED
										2.4×10^{-4}	4.1×10^{-3}	P3S03D9_SAT, P3S03D10_SAT[a], P3S03D11_SAT
0.053	0.50	1.1	0.041	0.0040	0.77	0.15	2.5×10^5	0.63	158	0.0	0.0	6 CW runs
										7.1×10^{-5}	8.7×10^{-4}	P3S05D1_LOW, P3S05D2_LOW, P3S05D8_LOW[a]
										2.1×10^{-4}	2.8×10^{-3}	P3S05D1_MED, P3S05D2_MED, P3S05D8_MED[a]
										4.1×10^{-4}	4.9×10^{-3}	P3S05D3_SAT[a], P3S05D4_SAT, P3S05D5_SAT
0.072	0.85	0.8	0.049	0.0061	0.876	0.16	2.9×10^5	0.70	216	0.0	0.0	6 CW runs
										9.6×10^{-5}	0.81×10^{-4}	P3S08D3_LOW[a], P3S08D7_LOW, P3S08D9_LOW
										3.2×10^{-4}	3.15×10^{-3}	P3S08D2_MED, P3S08D8_MED[a], P3S08D9_MED
										9.8×10^{-4}	9.4×10^{-3}	P3S08D2_SAT, P3S08D3_SAT[a], P3S08D5_SAT

Note: CW = clear water; LOW = lower concentration; MED = intermediate concentration; and SAT = full saturation; u_* = friction velocity; θ = Shields number; S = suspension number (w_s/u_*); Q = flow discharge; S_0 = slope of the channel; U = bulk mean velocity; H_f = water depth; Re = bulk Reynolds number; Re_* = Reynolds roughness number; Fr = Froude number; q_s = measured solid load per unit width; and $\bar{C}$ = measured depth-averaged volumetric concentration.
[a]Runs for which the profiles are presented.

intermediate (MED) solid load cases, respectively. Similar values of mean concentration below transport capacity were set for all three hydraulic forcing conditions. This procedure aims to investigate the effects of sediments on the turbulent boundary layer with gradual increase of concentration and to potentially isolate the effect of the turbulence level by comparing different forcing conditions for the same mean concentration.

The Acoustic Concentration and Velocity and Acoustic (ACVP) technology, combining acoustic Doppler velocity profiler (ADVP) with acoustic backscattering systems (ABS) technologies in a single flow instrumentation (Hurther et al. 2011), was used herein for the measurements. It provides colocated profiles along the bed-normal direction of streamwise and wall-normal velocity components, particle volumetric concentration, and particle flux across both the dense bedload and dilute suspension layers (Revil-Baudard et al. 2015, 2016; Fromant et al. 2018, 2019). Following the statistical convergence criteria proposed in Thorne and Hurther (2014) for incoherent particle scattering theory, the sampling frequency in the present study was set to 100 and 5 Hz for velocity and concentration, respectively. The operating acoustic frequency of 1 MHz, with a pulse duration of 2 μs leads to a vertical resolution of $\Delta z = 1.5$ mm. To minimize the flow intrusiveness, the ACVP sensors were placed into a vacuum box, with its lower end slightly below the free-surface level. Because the box disturbs locally the free-surface, the profiles presented herein are restricted to the lower 60% of the flow depth.

Three runs for each solid transport condition were acquired to confirm the repeatability of the results, leading to nine solid load runs for each hydraulic regime. This led to a total of 27 runs of sediment-laden flows for the three forcing conditions (see Supplemental Materials for more details). In general, most sequences of measurements included one CW run and only one or two SL runs. This resulted in a high number of clear-water runs (20 in total) obtained to cover all desired transport regimes. In the following, only one out of the three runs and its associated clear-water run, will be shown and discussed because the results showed a high degree of repeatability (Guta et al. 2020). Nevertheless, the range of variability of the main quantities over the three runs is given in Table 2. It will be seen that the deviations between the repeated runs remained below 10%, with very few exceptions that reached about 15%, which is very reasonable.

From the depth-averaged flow quantities presented in Table 1, the flow may be characterized as highly turbulent ($Re = 4UR_h/\nu \gg 2{,}000$, where R_h is the hydraulic radius, and ν is the kinematic viscosity), hydraulically rough (roughness Reynolds number: $Re_* = u_* k_s/\nu > 70$, with the following approximation for the roughness height $k_s \approx d_p$), and subcritical (Froude number: $Fr = U/\sqrt{gH_f} < 1$). Further details about the flow conditions for each experimental run are presented in Table S1 of the Supplemental Materials. For all the SL runs, the Shields number θ is always approximately equal or larger than 0.3 ($\theta \geq 0.35$) whereas the suspension number values cover the transitional regime ($0.8 < S < 1.0$) between suspension and no-suspension mode for the two most energetic hydraulic conditions and the no-suspension mode ($S = 1.3$) for the less energetic flow condition. This implies that for the two most energetic hydraulic conditions (under full transport capacity), bedload and suspended particle transport rates are both significant whereas bedload should largely dominate for the less energetic hydraulic condition. The large particle size $d_p = 3$ mm with low density is chosen in order to generate large bedload thicknesses in the 0 (1–2 cm) range. This allows for turbulence resolved measurements with the ACVP technology across both the bedload and suspension-load layers.

Results

In this section, the results are first presented in terms of hydrodynamic and sediment transport quantities (subsection "Mean Flow and Solid Transport Profiles"). Then, the vertical flow structure of SL flows are analyzed with a focus on the turbulence dominated suspension layer for the mixing length (subsection "Turbulent Mixing Length"), the velocity profile (subsection "Velocity Distribution"), and the concentration distribution (subsection "Concentration Distribution"). Finally, the depth-averaged ratio of turbulent particle diffusivity ϵ_s and eddy viscosity ϵ_{ms}, known as the β-factor (van Rijn 1984; Dey 2014), is presented in the last subsection. Please note that the analysis of the internal structure of the bedload layer was previously presented in Revil-Baudard et al. (2015), considering intergranular stresses due to particle collisions and frictional interactions. These aspects are not investigated herein.

Mean Flow and Solid Transport Profiles

To illustrate the novelty of the present experimental data set for studying SL flows, Fig. 2 shows several mean hydrodynamic quantities obtained for saturated (upper row), moderate (second row), low (third row) particle load conditions, and clear-water flow condition (bottom), each symbol represents a different hydraulic

Table 2. Summary of results, including range of variation over different experimental runs

u_* (m/s)	Θ	q_s ($\times 10^{-4}$) (m^2/s)	$\bar{C}$ ($\times 10^{-3}$)	κ_s	δ/d_p	z_d/d_p	β
0.044	0.35	0.0	0.0	0.40 ± 0.01	—	0.50 ± 0.2	—
		0.67 ± 0.04	1.20 ± 0.07	0.38 ± 0.01	4.70 ± 0.58	2.79 ± 0.26	2.42 ± 0.18
		1.42 ± 0.07	2.60 ± 0.09	0.37 ± 0.02	5.70 ± 0.30	3.65 ± 0.20	2.36 ± 0.71
		2.42 ± 0.16	4.10 ± 0.26	0.31 ± 0.04	6.03 ± 0.40	3.28 ± 0.23	2.90 ± 0.10
0.053	0.50	0.0	0.0	0.4 ± 0.01	—	0.30 ± 0.2	—
		0.71 ± 0.09	0.87 ± 0.15	0.39 ± 0.01	4.52 ± 1.00	1.69 ± 0.23	2.26 ± 0.39
		2.17 ± 0.11	2.80 ± 0.14	0.38 ± 0.01	5.70 ± 0.58	2.68 ± 0.23	2.33 ± 0.21
		4.06 ± 0.27	4.90 ± 0.38	0.35 ± 0.02	6.89 ± 0.77	3.13 ± 0.41	2.20 ± 0.51
0.072	0.85	0.0	0.0	0.40 ± 0.01	—	0.10 ± 0.2	—
		0.96 ± 0.09	0.81 ± 0.10	0.40 ± 0.03	2.17 ± 0.29	0.12 ± 0.27	1.71 ± 0.31
		3.15 ± 0.14	3.15 ± 0.05	0.36 ± 0.03	4.02 ± 0.87	1.15 ± 0.52	1.90 ± 0.28
		9.76 ± 0.51	9.40 ± 0.80	0.32 ± 0.04	7.21 ± 0.58	2.21 ± 0.72	2.21 ± 0.18

Note: κ_s = von Karman in sediment-laden flows; δ = bedload thickness; z_d = displacement height of the mixing length; and β = depth-averaged ratio between sediment and momentum diffusivity.

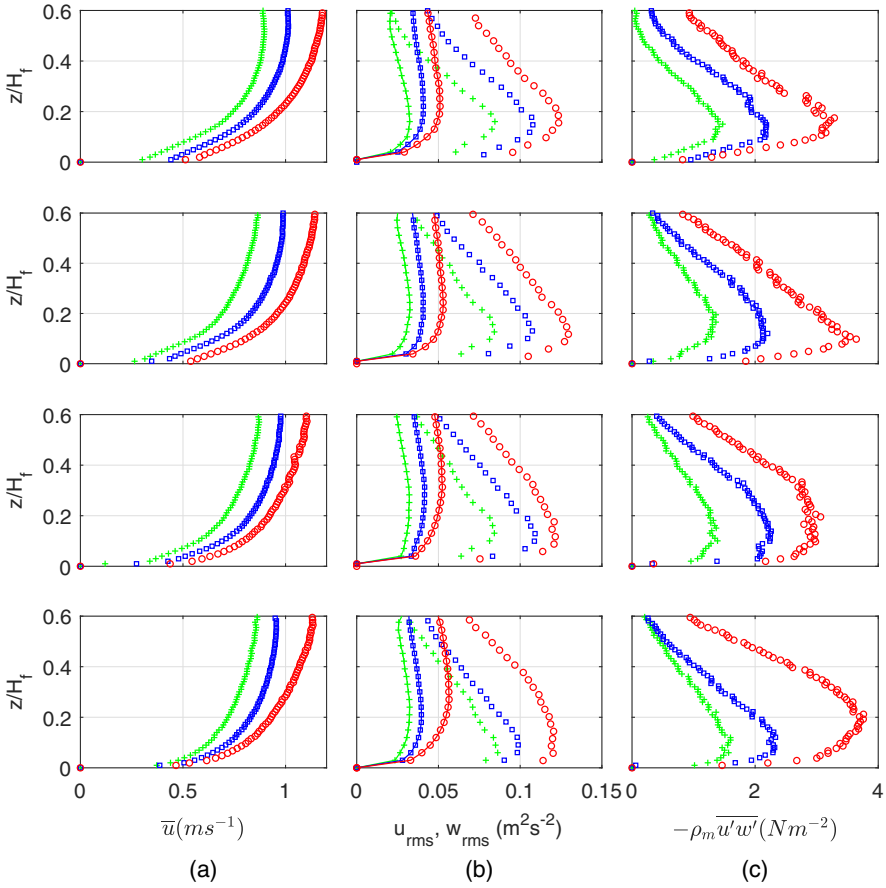

Fig. 2. Mean profiles of (a) velocity; (b) turbulent intensities (with marker for u_{rms}; marker and line for w_{rms}); and (c) Reynolds shear stress for $\theta \approx 0.35$ (×), $\theta \approx 0.50$ (square), and $\theta \approx 0.85$ (circle); increasing concentration from clear water (bottom row) to near saturation (top row).

condition (see Table 1). Fig. 2(a) shows the mean streamwise velocity ū profiles with flow-depth normalized distance z/H_f from the bed. For all conditions, the mean velocity profiles show the gradual increase in the hydrodynamic forcing with no clear evidence of particle load on the shape and magnitude of the velocity profiles in absolute values. Fig. 2(b) represents the turbulence intensity profiles for the longitudinal u_{rms} and vertical w_{rms} velocity components. Due to the inherent Doppler noise contribution affecting pulse-to-pulse coherent Doppler velocity measurements (Hurther and Lemmin 2001), the Doppler noise suppression technique of Garbini et al. (1982) is applied here. As expected for fully turbulent, steady uniform, and hydraulically rough open-channel flows, the clear-water flows shown in the lower panel reveal for all three hydraulic forcing conditions, a turbulence intensity profile of much lower magnitude for the vertical component than for the streamwise component. Its maximal value close to the bed is more than two times smaller. This strong near-bed turbulence anisotropy is typical for highly turbulent rough-bed open-channel flows (Nezu and Nakagawa 1993). As can be seen in Fig. 2(b) for the SL flows, no clear influence of the presence of particles can be distinguished on the magnitude and shape of the turbulence intensities profiles. The profiles of turbulent Reynolds shear stress, $\rho_m\overline{u'w'}$ where $\rho_m = (1-\bar{c})\rho_f + \bar{c}\rho_p$ is the mixture density, are shown in Fig. 2(c). For all flow conditions, the profiles show a linear behavior for $z/H_f > 0.2$, although small deviations are observed particularly in full capacity. This behavior reveals the high degree of flow uniformity in streamwise direction (Kironoto and Graf 1994; Dey 2014). The bed friction velocity given in Table 1 is estimated from the linear extrapolation of these profiles to the flow bed position ($z = 0$) with an uncertainty on u_* of about 10%. It can be seen that the bed-shear stress of the most energetic flow regime is approximately twice that of the less energetic one. Despite minor differences in profile shapes and maxima location inside the inner flow region ($z/H_f < 0.2$), the values of bed friction velocity do not vary more than 20% between CW and SL flows and it does not exhibit clear trends. It should be mentioned that the presence of the ACVP holding box affects the distribution of the shear stress profiles in the upper flow region for $z/H_f > 0.6$.

Fig. 3 presents mean particle transport quantities from lower concentration (bottom row) to capacity conditions (upper row). The time-averaged concentration $\bar{c}$ profiles shown in Fig. 3(a) confirm the increase in particle loading from the lower to the upper panels. Moreover, for a similar mean particle concentration, the differences in particle distribution over depth with hydraulic forcing condition can be analyzed. It can be seen that the vertical extension of the concentration profile decreases with increasing w_s/u_* [cross symbol curves in Fig. 3(a) represent the flow with highest suspension number w_s/u_*] confirming that less particles are transported in suspension compared to the cases of lower suspension number values [circle and square symbol curves in Fig. 3(a)]. The corresponding concentration profile for the high suspension number value exhibits higher vertical gradients originating probably from less turbulent particle concentration mixing (see section "Concentration Distribution"). Fig. 3(b) shows the profiles of sediment flux density $\pi(z) = \bar{u}(z) \times \bar{c}(z)$ in streamwise direction. As expected, the most energetic flow conditions (circle symbol) in

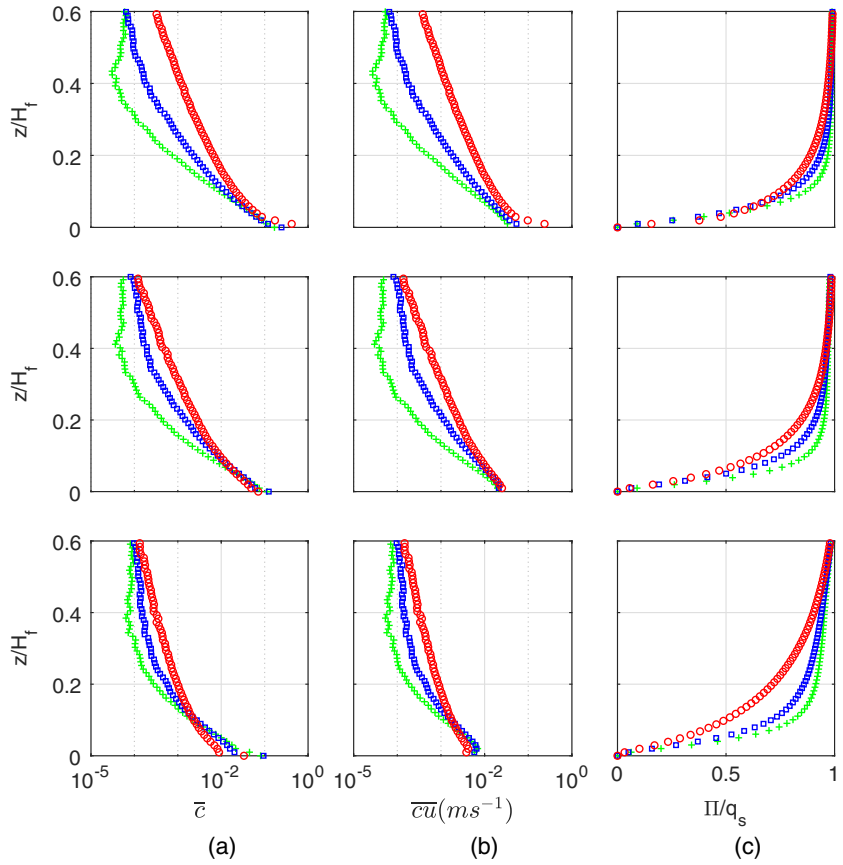

Fig. 3. Mean profiles of (a) concentration; (b) sediment flux; and (c) normalized cumulative sediment flux for $\theta \approx 0.35$ (×), $\theta \approx 0.50$ (square) and $\theta \approx 0.85$ (circle); increasing concentration from low (bottom row) to near saturation (top row).

capacity conditions (upper panels) carries more particles due to its higher bed-shear stress and higher flow velocities. This is not only true close to the bed but also far from the bed, in the outer flow region, corresponding to the suspension layer. In order to quantify directly the relative contribution of bedload and suspended particle transport as a function of hydraulic forcing and particle load, Fig. 3(c) represents the cumulative sediment flux $\Pi(z)$ in streamwise direction (normalized by the total solid flux)

$$\Pi(z) = \int_0^z \pi(z)dz \tag{1}$$

It can be seen from the capacity conditions (upper panels) that the less energetic flow (highest suspension number w_s/u_*, represented by the cross symbol curve) carries more particles close to the bed as bedload than in the more dilute region as suspended load. For the more energetic flow conditions corresponding to lower w_s/u_* values, more particles are transported as suspended load. The sheet-flow regime is prevalent mostly in capacity conditions. At lower solid loads, a larger proportion of transport occurs in suspension, inhibiting the development of the bedload layer, particularly for lower suspension numbers ($w_s/u_* < 1$). In the following, the term sheet flow will be used without distinction in degree of saturation.

Turbulent Mixing Length

The law of the wall is based on two basic assumptions: in the wall region of a fully turbulent wall-bounded flow, the turbulent mixing length is proportional to the distance z from the bed and the shear stress is nearly constant, which can be approximated by the bed-shear stress $\tau = \tau_0 = \rho u_*^2$. Measured profiles of Reynolds shear stress follow a nearly constant trend for $0.10 \le z/H_f \le 0.30$ around the maximum values and a nearly linear mixing length profile $[l_{ms} = u_*/(du/dz)]$ for $(z/H_f) \ge 0.05$–0.15, as can be seen in Figs. 2(c) and 4, respectively. Please note that the nearly constant trend of the measured Reynolds stress profiles ($0.10 \le z/H_f \le 0.30$) herein refers to the region around its maximum value, in which variations lower than 20% from the maximum are observed; hence, $\sqrt{|\overline{u'w'}|}$ can be approximated as u_* following Prandtl assumption. In the near-bed region, corresponding to $(z/H_f) \le 0.05$–0.15, Fig. 4 reveals that the mixing length profiles for all SL flows deviates from the linear distribution.

The level δ below which the measured mixing length deviates by more than 15% from the linear fit is arbitrarily defined as the bedload layer thickness. This threshold matches roughly the accuracy of the mixing length measurements (10%–15%). The upper limit of the linear fit was limited such that the squared correlation coefficient between the fitted and measured data remained higher than 90% ($R^2 \approx 0.9$). Above the vertical level δ, the mixing length follows the linear relationship

$$l_{ms} = \kappa_s(z - z_d) \tag{2}$$

where z_d = level corresponding to the origin of the (linear) fitted mixing length; and κ_s = von Karman constant in SL flows. The level δ, illustrated with a horizontal dashed line in Fig. 4, corresponds to the transition between the turbulence dominated region

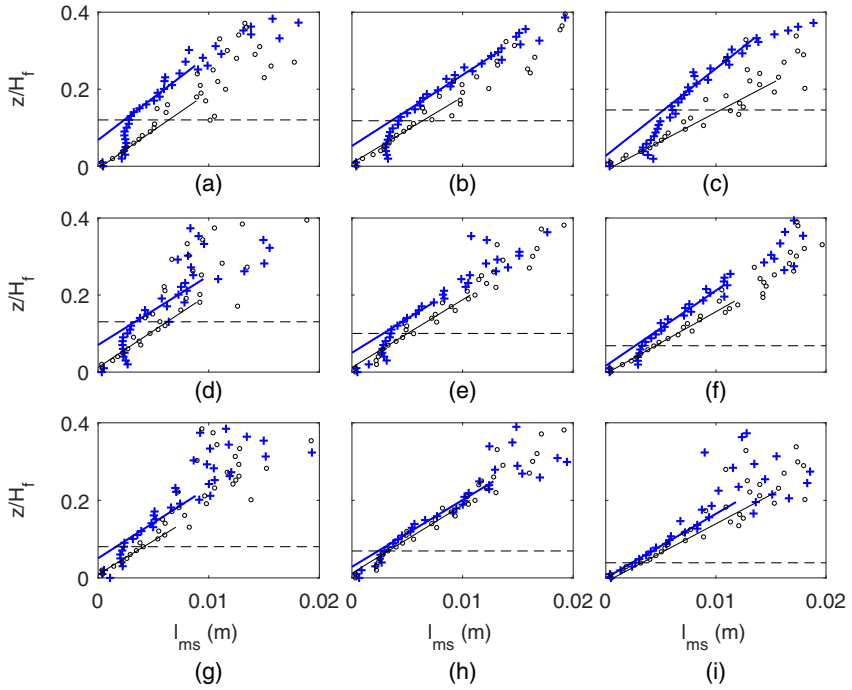

Fig. 4. Mixing length for saturated concentration (first row): (a) $\theta \approx 0.35$; (b) $\theta \approx 0.50$; and (c) $\theta \approx 0.85$; intermediate concentration (second row): (d) $\theta \approx 0.35$; (e) $\theta \approx 0.50$; and (f) $\theta \approx 0.85$; and lower concentration (third row): (g) $\theta \approx 0.35$; (h) $\theta \approx 0.50$; and (i) $\theta \approx 0.85$. Plus symbol (+) is for sediment-laden and circle is for clear water. Dashed line corresponds to bedload thickness δ.

or suspension layer and the particle-particle interaction dominated region defined as the bedload layer. Based on the considerations proposed by Bagnold (1956), Wilson (1987, 1989) reported that the thickness of this layer is approximately $\delta/d_p \approx 10\theta$. This should be taken as an indicative value, as Sumer et al. (1996) argued that the dynamics of sheet-flow processes depend on whether the sheet-flow is in suspension, transitional, or no-suspension regime. Furthermore, Ribberink et al. (2008) showed that the proportionality constant 10 can also vary by more than 30% due to the different methods applied by authors for the bedload layer thickness estimation. This is confirmed herein, with the proportionality constant in capacity conditions, having values of 17, 12.5, and 9 for the three flow regimes reported herein (from lower to higher Shields number), based on the linear mixing length criteria. The corresponding bedload thickness are $\delta \approx 6d_p$, $6.5d_p$, and $7d_p$, respectively. Note that the agreement with the proportionality constant of 10 is particularly good for the most energetic flow conditions, which are closer to the conditions in which this parametrization was obtained ($\theta \geq 1$). The result also agrees well with Sumer et al. (1996) for their larger particle experiments (designated Sediment 1 and 2 in their manuscript), with a range of bedload thickness of $(\delta/d_p) \approx 5$–15. Due to the large size and the low density of the particles used in the present work, the bedload layer of all studied SL flows is considerably thick and can be well resolved by the ACVP measurement, since $\delta/z_d = 7$ corresponds roughly to $z/H_f \approx 0.14$. Recently, Blanckaert et al. (2017) estimated the bedload thickness based on ADVP measurements and obtained a value of $\delta/d_p \approx 10$ for their most intense flow conditions. This value is consistent with the present results.

Applying the proposed criteria, the proportion of bedload/suspended load evolves from approximately 20%/80%, 40%/60%, and 70%/30% to 70%/30%, 80%/20%, and 90%/10% as the concentration is increased from low sediment load to capacity, for $w_s/u_* = 0.8$, 1.0, and 1.3, respectively. The only regime persistently displaying a greater proportion of bedload is the one with $w_s/u_* \approx 1.3$, independently on the particle transport rate. This confirms that we are in presence of a bedload dominated regime [named the no-suspension regime after Sumer et al. (1996)], and two transitional regimes in which greater proportions of suspended load occur at lower concentration, while greater proportion of bedload occurs in saturation.

Another relevant quantity is the displacement height z_d defined as the origin of the linear mixing length profile [Eq. (2)]. Sumer et al. (1996) found that as the bedload thickness, z_d, also increases with Shields number θ, and its magnitude was approximately $0.5\delta < z_d < \delta$. This is in good agreement with the present experiments in capacity conditions for which $0.4\delta < z_d < 0.7\delta$.

For the highest sediment load experiments, the mixing length values are larger than the one measured in the corresponding CW flow inside the bedload layer for $z/H_f \leq 0.05$ (circle symbol curves in Fig. 4). This supports the existence of additional shear stress due to particle-particle interactions. Nevertheless, since the mixing length remains nearly constant over the entire bedload layer, the clear-water value exceeds this constant value at a certain height inside the bedload layer because its linear trend starts from a level much closer to the bed. The slope of the mixing length in SL flow gradually converges to CW values, above the bedload layer. The obtained values of κ_s estimated from the linear fit of the mixing length are quite close to CW values for lower and intermediate concentrations, and moderately smaller for the highest sediment loads (see Table 2). It implies that in the present conditions, the absolute value of the mixing length at a given vertical level in the suspension layer may be significantly reduced, due principally to the large displacement height z_d induced by the presence of the bedload layer rather than a strong reduction of mixing efficiency via a lower κ_s value. This is especially the case for moderate concentrations ($\bar{C} < 2 - 3 \times 10^{-3}$), as seen in Fig. 4. Revil-Baudard et al. (2016) also found a strong upshift of the linear mixing length profile

[see their Fig. 2(b)] due to a large displacement height associated with the bedload layer in agreement with the present results. However, a much lower κ_s value was measured in the turbulent suspension layer, which might be due to experiments conducted in fully developed capacity conditions over mobile granular beds.

The mixing length model is widely applied as a closure for velocity and concentration distribution through the eddy viscosity concept. Under the assumption of a constant Reynolds shear stress in the logarithmic layer and a linear profile in the above outer flow region [confirmed from Fig. 1(c)], the well-known parabolic distribution of eddy viscosity (Lyn 2008) is given by

$$\epsilon_{ms} = \kappa_s u_*(z - z_d)\left(1 - \frac{z}{H_f}\right), \quad \text{for } z > \delta \tag{3}$$

Eq. (3) is valid in the flow region where the mean velocity distribution follows a logarithmic profile, usually called the log-layer. Above the log-layer, several researchers (Coleman 1981; Nezu and Rodi 1986) have shown that a better agreement is found when wake effects are included using the log-wake law. These effects are not considered here since the wake region is affected by the presence of the ACVP holding box placed at the water free-surface. For this reason, no profile is analyzed in this study for $z/H_f \geq 0.6$. In the following two subsections, the immediate implications of the modified turbulent mixing length and eddy viscosity on mean velocity and concentration will be presented.

Velocity Distribution

The present section aims at proposing a revisited formulation of the mean velocity distribution valid in the suspension layer for SL flows of heavy particles. Integrating $du/dz = u_*/\kappa_s(z - z_d)$ in the suspension layer from the bedload layer thickness δ to a given position z, the velocity profile can be written as

$$u = \frac{u_*}{\kappa_s}\ln(z - z_d) + C \tag{4}$$

with $u = u_\delta$ at $z = \delta$, the integration constant is $C = u_\delta - u_*/\kappa_s \ln(\delta - z_d)$. Therefore, the law of the wall takes the following form:

$$u = \frac{u_*}{\kappa_s}\ln\left(\frac{z - z_d}{\delta - z_d}\right) + u_\delta \tag{5}$$

In the literature, the log-law in CW is often described with a similar equation, taking $u_\delta = B_r u_*$, where B_r is the integration constant valid for rough flows (Garcia 2008), and $\delta - z_d = k_s$ is the roughness height. The displacement height z_d also appears in CW for hydraulically rough flows due to the presence of a roughness sublayer. Herein, the displacement height z_d of SL flows is larger than in the respective CW flows. The velocity profile can be fitted to determine κ_s and B_r as the usual practice. The obtained values of κ_s are generally in very good agreement (not shown here) with those determined from the slope of the mixing length distribution (Fig. 4). This is consistent with the good agreement between Eq. (5), represented as solid lines in Fig. 5 with experimental data (cross symbols). The velocity profile is following closely the logarithmic distribution given by Eq. (5) over the entire suspension layer (above the vertical dashed line). Compared with the logarithmic layer in the corresponding CW flows (cross symbol and solid curves), it can clearly be seen that the log-layer in the sheet-flow conditions are strongly shifted upward due to the presence of the bedload layer. Inside the bedload layer, the velocity distribution approaches a quasi-linear shape in the vicinity of the fixed bed. A similar trend has been reported by Sumer et al. (1996), who parametrized the velocity profile with a power law having an exponent close to unity (0.75). Regarding the overall shape of the observed velocity profiles, there is a good agreement with previous literature results (Einstein 1955; Coleman 1981; Lyn 1988). Typically, a significant

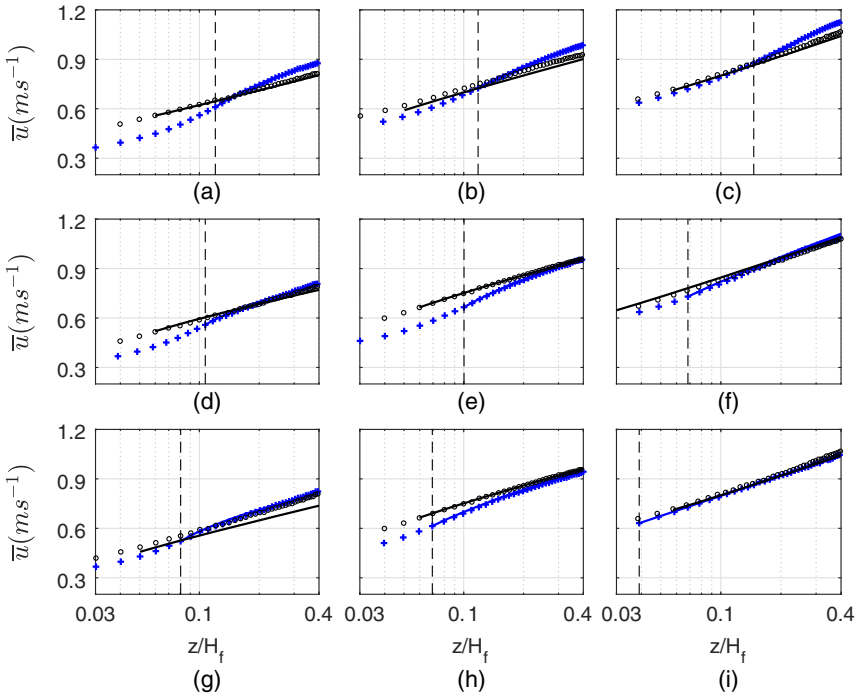

Fig. 5. Velocity distribution for SL (plus symbol) and CW (circle) for saturated concentration (first row): (a) $\theta \approx 0.35$; (b) $\theta \approx 0.50$; and (c) $\theta \approx 0.85$; intermediate concentration (second row): (d) $\theta \approx 0.35$; (e) $\theta \approx 0.50$; and (f) $\theta \approx 0.85$; and lower concentration (third row): (g) $\theta \approx 0.35$; (h) $\theta \approx 0.50$; and (i) $\theta \approx 0.85$. Solid line corresponds to Eq. (5) and dashed line corresponds to δ.

reduction of the flow velocity in the bedload layer followed by an increase in the outer layer is observed in the reported data when compared to the respective CW velocity profiles. A similar trend was recently found by Blanckaert et al. (2017).

Concentration Distribution

The present section aims at proposing a revisited formulation of the mean particle concentration distribution in the suspension layer of heavy SL flows. Following Rouse (1938) using the mass conservation equation for the sediment phase, the equation for concentration distribution can be obtained from the equilibrium between the upward ($\overline{c'w'} = \epsilon_s dC/dz$) and downward ($w_s C$) sediment fluxes

$$w_s C + \epsilon_s \frac{\partial C}{\partial z} = 0 \tag{6}$$

Rearranging, and taking $\epsilon_s = \beta \epsilon_{ms}$ one can write

$$\int_{C_a}^{c} \frac{dC}{C} = -w_s \int_{a}^{z} \frac{dz}{\beta \epsilon_{ms}} \tag{7}$$

where $\beta = \overline{\epsilon_s/\epsilon_{ms}}$. To obtain the concentration profile, Eq. (7) is usually integrated using the eddy viscosity in clear-water flows $\epsilon_{ms} = \kappa_s u_* z(1 - z/H_f)$, which yields the so-called Rouse equation

$$\frac{C}{C_a} = \left(\frac{H_f - z}{z} \frac{a}{H_f - a} \right)^{\frac{w_s}{\beta \kappa_s u_*}} \tag{8}$$

where C_a = reference concentration taken at a level $z = a$ inside the suspension layer. It is traditionally taken as $a \approx 0.05 H_f$ or $a \approx 2d_p$ (García 2008). The exponent $Z_R = w_s/(\beta \kappa_S u_*)$ is often referred to as the Rouse number. It shall be recalled here that the Rouse profile is valid only in the dilute suspension layer. Moreover, the prescription of a distribution of ϵ_{ms} based on the linear mixing length model implies that, strictly, it should only be valid in the log-layer. Extending its range of validity to the outer flow region of an open-channel flow requires consideration of the log-wake law for ϵ_{ms} as referred to previously (see subsection "Turbulent Mixing Length"). In the present SL flow conditions, it is found that the prescribed CW eddy viscosity profile strongly differs from the one proposed in Eq. (3). Indeed, for the classical eddy viscosity profile, no effect of the displacement height due to the presence of the bedload layer is accounted for. If the effect of the upshift of the log-layer is included, as described in Eq. (3), the solution of Eq. (7) becomes

$$\frac{C}{C_a} = e^{-Z_r \left[\frac{2}{F} a \tan\left(\frac{-2z/H_f + B}{F} \right) - a \tan\left(\frac{-2a/H_f + B}{F} \right) \right]} \tag{9}$$

where

$$F = \sqrt{\frac{4 z_d}{H_f} - \left(1 - \frac{z_d}{H_f} \right)^2} \tag{10}$$

and

$$B = \left(1 - \frac{z_d}{H_f} \right) \tag{11}$$

are two integration constants.

The β-factor can be determined experimentally taking ϵ_s estimated using Eq. (6) and $\epsilon_{ms} = -\overline{u'w'}/(du/dz)$. The β value corresponds to the depth-averaged value of ϵ_s/ϵ_{ms} over the range of quasi-constant magnitude found in the suspension layer as it will be shown later. The behavior of this crucial parameter and its prediction from a model will be addressed in the following subsection. The reference concentration is not taken at $a \approx 0.05 H_f$ or $a \approx 2d_p$, as classically done, since the bedload layer thickness varies considerably as a function of SL flow conditions (see subsection "Turbulent Mixing Length"). The reference height here will be taken as the value of the bedload thickness $a = \delta$. This will allow to test the validity of the new suspended sediment concentration formulation over the largest possible vertical range. The comparison between the measured and predicted concentration profiles from Eq. (9) and from the classical Rouse equation [Eq. (8)] are represented in Fig. 6. The measured concentration distribution is well described by the revisited analytical solution. Note that the agreement is consistently better for the four panels [Figs. 6(b, c, e, and f)] in which higher suspension load occurs. Although a relatively good agreement prevails, greater relative differences between the modeled and measured profiles are observed in the cases with the lowest concentrations or proportion of suspended load. This trend may indicate that high accuracy is required to model very low concentrations. One can observe that the Rouse equation overestimates the concentration profile, consistent with the higher eddy viscosity model. Both equations provide good results when z_d is small. This is seen for the low concentration of the strongest flow regime [Fig. 6(i)] for which most of the sediment load is carried in suspension. In this case, the bedload thickness δ is small, with a value of $z/H_f \approx 0.05$ very close to the reference height usually taken in open-channel suspension flows ($w_s/u_* < 0.8$). In cases in which a thick bedload layer exists, the arbitrary height of 5% relative to the local flow depth might be located inside the bedload layer, inducing significant errors in concentration prediction when using the classical Rouse formulation. In the present study, the new formulation of the suspended sediment concentration profile offers improved sediment transport prediction over the entire suspension layer in flows in which both bedload and suspended load are significant (i.e., $0.6 < w_s/u_* < 1.5$).

Ratio of Sediment and Momentum Diffusivities: The β-factor

The depth-averaged ratio between sediment and momentum diffusivity, β-factor, enters into the analytical solution for the mean suspended concentration profile via the Rouse number, as shown in the previous subsection. Fig. 7 shows the vertical distribution of β as well as the depth-averaged value over the quasi-constant vertical range. As can be seen, the assumption of proportionality between ϵ_s and ϵ_{ms} over the suspension layer is well justified. For the less energetic hydraulic condition [Figs. 7(a, d, and g)] exhibiting a high variability in β-values, the larger discrepancies can be explained by the high suspension number $w_s/u_* = 1.3$, supporting a bedload dominated transport regime. Furthermore, we can see that the variability in β-values is reduced for all other cases with increasing sediment load. This can be attributed to the increase of suspended particle concentration with loading whereas for the less energetic flow regime with a value of $w_s/u_* = 1.3$, the amount of suspended particles remains low even for the highest injected particle load due to the bedload dominated transport regime. The β-factor values show a weak dependence on concentration for all flow conditions, which is in good agreement with previous direct measurements reported by Cellino and Graf (1999) obtained in fully suspended ($w_s/u_* < 0.6$) sediment-laden open-channel flows.

The evolution of β-values with suspension number $S = w_s/u_*$ is shown in Fig. 8 for all studied SL flows together with some existing literature data and the empirical model of van Rijn (1984) given by Eq. (12) (solid line)

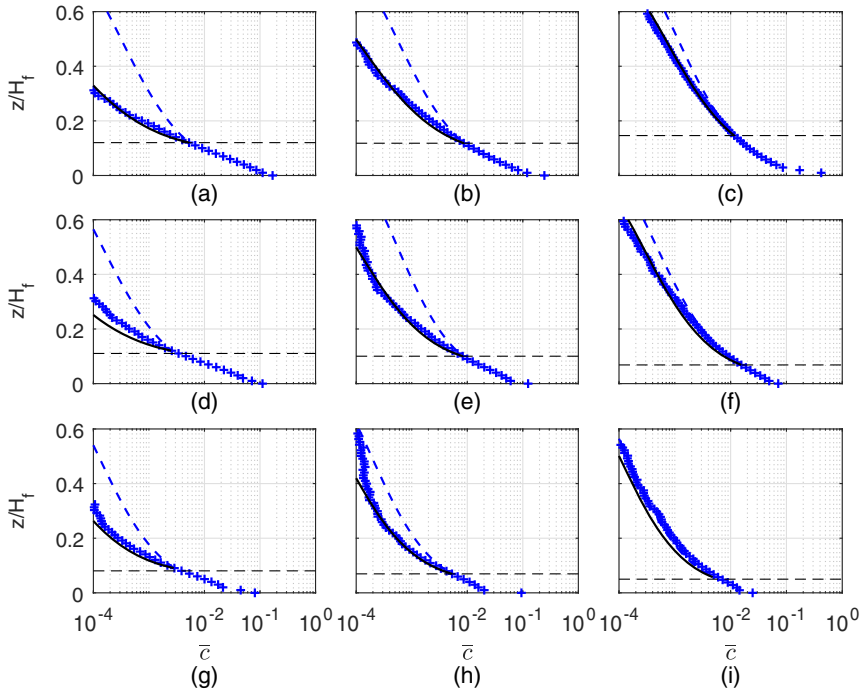

Fig. 6. Concentration distribution for measured (plus symbol), Rouse profile (widely spaced dashed line) as in Eq. (8), and modified Rouse profile (dashed line) as in Eq. (9) for saturated concentration (first row): (a) $\theta \approx 0.35$; (b) $\theta \approx 0.50$; and (c) $\theta \approx 0.85$; intermediate concentration (second row): (d) $\theta \approx 0.35$; (e) $\theta \approx 0.50$; and (f) $\theta \approx 0.85$; and lower concentration (third row): (g) $\theta \approx 0.35$; (h) $\theta \approx 0.50$; and (i) $\theta \approx 0.85$.

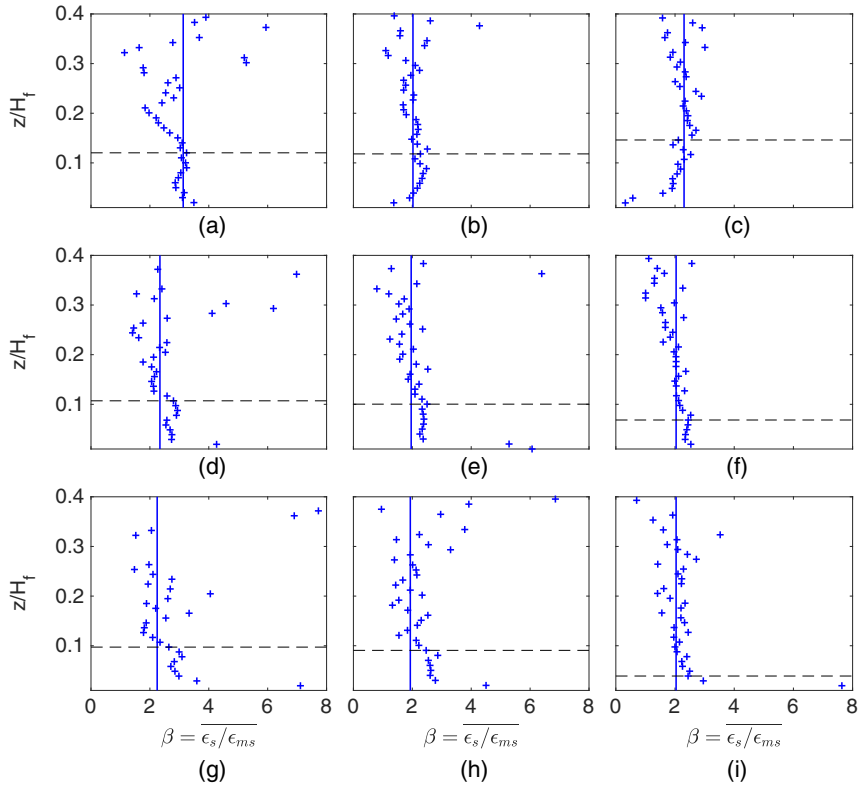

Fig. 7. Ratio of sediment and momentum diffusivity and its depth-averaged value β for saturated concentration (first row): (a) $\theta \approx 0.35$; (b) $\theta \approx 0.50$; and (c) $\theta \approx 0.8$; intermediate concentration (second row): (d) $\theta \approx 0.35$; (e) $\theta \approx 0.50$; and (f) $\theta \approx 0.8$; and lower concentration (thrid row): (g) $\theta \approx 0.35$; (h) $\theta \approx 0.50$; and (i) $\theta \approx 0.8$.

$$\beta = 1 + 2\left(\frac{w_s}{u_*}\right)^2 \quad \text{for } 0.1 < w_s/u_* < 1 \tag{12}$$

A reasonable agreement with the model is found for $w_s/u_* < 1$, which corresponds to the SL flow conditions used to derive the model. The present data are in reasonable agreement with experimental results from Barton and Lin (1955), Coleman (1970), and Muste et al. (2005). Among the analyzed data, measurements from Lyn (1988) are the only to display the opposite trend (β decreases with w_s/u_*), with values rather close to unity ($\beta \approx 0.83 - 1.16$). Graf and Cellino (2002) also observed increasing β-values with w_s/u_*, but with values systematically below unity ($\beta \approx 0.5$). This can be attributed to the methodology applied for the calculation of the β-factor based on direct measurement of $\overline{c'w'}$ rather than Cw_s (applied herein and in most other studies). Nikora and Goring (2002) used the same method as Graf and Cellino (2002) to estimate β, and the authors obtained values close to unity or slightly above it (not shown here). Their experiments had very low suspension numbers ($w_s/u_* < 0.1$) supporting the convergence of β toward unity for very small particles having very low inertia relative to the surrounding fluid parcels. A modification of van Rijn (1984) model is proposed here [Eq. (13)] to extend the model over a wider range of suspension numbers

$$\beta = 1 + 0.7\left(\frac{w_s}{u_*}\right) + 0.7\left(\frac{w_s}{u_*}\right)^2 \quad \text{for } 0 < w_s/u_* < 1.5 \tag{13}$$

Discussion

Bedload layer effects on the velocity distribution in a SL flow involving heavy particles have been reported herein and a modified velocity distribution model has been proposed in Eq. (4), which takes these effects into account. As shown throughout its derivation, this modified logarithmic solution is valid only above a certain distance from the bed, herein corresponding to the top of the bedload layer, in which the linear mixing length assumption becomes valid. Sumer et al. (1996) noticed in their sheet-flow experiments with their largest particles, having similar particle diameters and density as in the present study, that the displacement height z_d may be much higher than the classical value for CW rough-bed flows. Furthermore, several researchers (Wilson 1989; Sumer et al. 1996; Ribberink et al. 2008) found that under sheet-flow conditions, the relative roughness scale is neither that from smooth (viscous length related) or rough flows (related to size of elements constituting the bed skin friction). As seen in Eq. (4), the thickness of the bedload layer δ and the displacement height z_d becomes the relevant length scale for defining k_s in SL flows involving heavy particles. This complex interaction between the bedload and the flow resistance was also highlighted by Camenen et al. (2006) and Recking et al. (2008) over wide range of flow and transport conditions.

One important outcome of the bedload layer induced upshift of the log-layer is the strong reduction of the mixing length in the near-wall region, and the classical analytical Rouse solution for the suspended particle concentration profile becomes inaccurate with increasing displacement height z_d (scaling with the bedload layer thickness). This seems to be due to the overestimation of the momentum diffusivity (and sediment diffusivity) in presence of a thick bedload layer. An inspection of Eq. (7) indicates that an overestimation of ϵ_{ms} leads to artificially reduced values of β, such that $\epsilon_s = \beta\epsilon_{ms}$ remains constant. It was indeed observed (not shown here) that the values of β obtained from a classical best fit method of the Rouse profile are systematically lower than those measured directly and represented in Fig. 8. On the contrary, a good

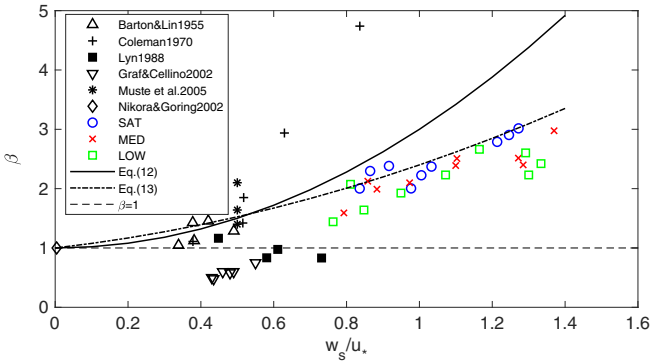

Fig. 8. Values of depth-averaged ratio of sediment and momentum diffusivity β as function of w_s/u_*. (Data from Lyn 2008.)

agreement was found between β values obtained from a best fit of the proposed modified Rouse solution [Eq. (9)] and the directly measured ratio $\beta = \epsilon_s/\epsilon_{ms}$. This confirms that in energetic SL flows and in presence of a thick bedload layer, β cannot be determined from a best fit of the classical Rouse equation as is usually done in laboratory and field studies.

In the subsection "Turbulent Mixing Length", it was shown that even at the lowest concentration investigated herein, the hydraulic regime with higher values of w_s/u_* (higher proportion of bedload) exhibited significant reduction of turbulent mixing length compared with the corresponding CW flows, although with similar values of κ_s. Since this reduction was due to larger displacement height z_d, it tends to indicate that the presence of a thick bedload layer is the dominant effect on the reduction of momentum mixing at moderate concentrations ($\bar{C} < 2 - 3 \times 10^{-3}$). With a higher suspended load, additional effects dependent on local concentration may also play a role in the damping of momentum mixing. This reduction of momentum mixing has been studied in the literature (Smith & McLean 1977; van Rijn 1984; Hsu et al. 2004) and a damping factor ϕ corresponding to the ratio between the eddy viscosity or turbulent mixing length in SL flows and the corresponding CW quantity has been introduced $\phi = \overline{\epsilon_{ms}/\epsilon_m}$. Fig. 9 shows the mean values of ϕ as a function of suspension number w_s/u_*, which have been depth averaged over the suspension region in the same way as the β-factor. It can be seen that ϕ slightly increases before decreasing around the critical value of about $S = w_s/u_* \cong 1$, regardless of the injected sediment load. Note that the observed trend of lower values of ϕ for higher suspension numbers, $w_s/u_* = 1.2$–1.3 seems to be well established for all concentrations. This is not as well established for the lower values of $w_s/u_* \leq 1$,

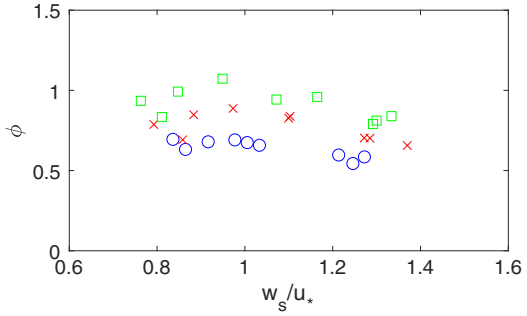

Fig. 9. Values of ratio of eddy viscosity in SL and corresponding CW flow: $\phi = \overline{\epsilon_{ms}/\epsilon_m}$. Circle = saturated concentration; × = intermediate concentration; and square = lower concentration.

particularly for saturated cases. Nevertheless, the change in trends of ϕ at roughly $w_s/u_* \cong 1$, suggests that different transport mechanisms occur in suspension and no-suspension mode. Furthermore, the combination of global effects (roughness and thick bedload layer) and local effects (stratification, drag modification, etc.) induces great challenges for two-phase flow modeling.

Summary and Conclusions

Bedload effects on turbulent suspension properties are investigated in SL flows involving heavy particles based on a new set of high-resolution experimental data. Turbulent particle transport processes were studied in laboratory open-channel flows under clear water, noncapacity, and capacity conditions, for three hydraulic regimes varying from $\theta \approx 0.35$ ($w_s/u_* \approx 1.3$) to $\theta \approx 0.85$ ($w_s/u_* \approx 0.8$). A new criterion for separating the bedload layer from the suspension layer has been proposed based on the vertical distribution of turbulent mixing length. Inside the suspension layer, the mixing length follows a linear profile with a von Karman constant as the proportionality factor, of value close to its clear-water flow value. Inside the bedload layer, the mixing length exhibits a quasi-constant vertical distribution as previously observed in Revil-Baudard et al. (2015, 2016). This criterion is found to be consistent with the signature of the other quantities such as the deviation of the velocity profile from the logarithmic distribution in the bedload layer. The results agree with the parametrization of Wilson (1987, 1989) for the bedload thickness δ in sheet-flow regime, only for the highest values of θ. The referred relationship seems to be adapted for high Shields number $\theta \geq 1$. For sheet-flow regime in the range $\theta < 1$ and $w_s/u_* > 1$, experimental results presented herein and previously in Sumer et al. (1996) may be indicative for the magnitudes of δ and z_d. Detailed analysis of bedload processes are necessary in order to provide more insights concerning the behavior of these parameters.

The logarithmic velocity profile layer occurs much higher in the water column due to the presence of the bedload layer. Indeed, for low to moderate concentrations (below capacity), a reduction in momentum mixing can be explained mainly by a modified origin z_d (displacement height) of the linear mixing length. A reduction in the von Karman constant as the slope κ_s (up to 25%) of the mixing length profile was observed for the highest concentrations, only over a limited vertical range. Indeed, κ_s gradually converges to its clear-water value with the gradual vanishing of of turbulence damping induced by the presence of particles. The modified mixing length and eddy viscosity profiles were subsequently applied to model velocity and suspended particle concentration in heavy particle sheet flows.

It was shown that the logarithmic velocity profile holds if applied above the bedload layer. Additional parameters that describe the thickness of the bedload layer δ and the origin z_d of the linear mixing length profile are taken into account in the law of the wall. Concerning the concentration distribution, it was shown that the classical Rouse equation becomes less accurate as the bedload layer thickness increases. This is due to the poor description of the classical eddy viscosity profile. Using the modified eddy viscosity (that includes the bedload layer induced upshift), a modified analytical solution for the profile of suspended particle concentration is proposed. It is shown that the new equation provides much better agreement than the classical Rouse formulation. When the bedload layer becomes negligibly small (i.e., when $S < 0.8$) the new model is consistent with the Rouse profile.

The quasi-proportionality between momentum and sediment diffusivity was verified. The determined values of β agree with the model of van Rijn (1984) at low suspension numbers ($0.1 < w_s/u_* < 0.8$). For larger values of the suspension number, van Rijn's model deviates from the presented data. A modified parametrization was proposed, such that it is applicable over a wider range of suspension numbers ($0 < w_s/u_* < 1.5$). Finally, it was seen that the damping in the momentum mixing relative to its corresponding clear-water ϕ is highly dependent on the turbulence level w_s/u_* and on the concentration. A transition in the evolution of the ϕ-factor is seen to occur at $w_s/u_* \approx 1$, supporting that different turbulent transport mechanisms occur in the suspension and no-suspension modes of heavy particle sheet flows.

The experimental data presented in this work will be a very valuable source of information for the development of multiphase flow models and the understanding of turbulence-particle interactions in sediment transport.

Data Availability Statement

All the data presented in this manuscript are freely available on zenodo and on the LEGI opendap server at the following address: http://servdap.legi.grenoble-inp.fr/opendap/meige/15SHEET_FLOW/.

Acknowledgments

The Project ANR SHEET-FLOW, granted by Agence Nationale de la Recherche (ANR), has funded the experiments and part of the first author PhD Thesis. The remaining financial support was granted through a Doctoral Scholarship by the French Ministry of Foreign Affairs.

Notation

The following symbols are used in this paper:

a = reference level for Rouse profile;
B = integration constant;
B_r = integration constant;
C = local time-averaged volumetric concentration;
C_a = reference concentration;
$\bar{C}$ = depth-averaged volumetric concentration;
C^{inj} = depth-averaged injected volumetric concentration;
d_p = particle median diameter;
F = integration constant;
Fr = Froude number;
g = gravitational acceleration;
H_f = water depth;
k_s = roughness height;
l_m = mixing length in clear-water flows;
l_{ms} = mixing length in sediment-laden flows;
Q = flow discharge;
Q_s^{inj} = mean injected solid load;
q_s = measured solid load per unit width;
Re = bulk Reynolds number;
Re_* = Reynolds roughness number;
R_h = hydraulic radius;
S = suspension number;
S_0 = bed slope;
U = bulk mean velocity;
u_{rms} = streamwise turbulence intensity;
u_* = shear velocity;
u_δ = streamwise velocity at the level $z = \delta$;

u' = streamwise velocity fluctuation;
w_s = settling velocity in still water;
w_{rms} = vertical turbulence intensity;
w' = vertical velocity fluctuation;
z = vertical coordinate;
z_d = displacement height (origin of linear mixing length);
β = depth-averaged ratio of sediment and momentum diffusivities;
δ = thickness of bedload layer;
θ = Shields number;
ϵ_m = eddy viscosity in clear-water flows;
ϵ_{ms} = eddy viscosity in sediment-laden flows;
ϵ_s = sediment diffusivity;
κ = von Karman constant in clear-water flow;
κ_s = von Karman constant in sediment-laden flow;
ν = kinematic viscosity;
ρ_f = water density;
ρ_m = mixture density;
ρ_p = sediment density;
τ = local shear stress;
τ_0 = bed-shear stress; and
Φ = depth-averaged ratio between eddy viscosity in SL and CW.

Supplemental Materials

Table S1 is available online in the ASCE Library (www.ascelibrary.org).

References

Bagnold, R. A. 1956. "The flow of cohesionless grains in fluids." *Philos. Trans. R. Soc. London. Ser. A, Math. Phys. Sci.* 249 (964): 235–297. https://doi.org/10.1098/rsta.1956.0020.

Barton, J. R., and P. N. Lin. 1955. *A study of the sediment transport in alluvial streams*. Rep. No. 55JRB2. Fort Colins, CO: Colorado A&M College.

Blanckaert, K., J. Heyman, and C. D. Rennie. 2017. "Measuring bedload sediment transport with an acoustic doppler velocity profiler." *J. Hydraul. Eng.* 143 (6): 04017008. https://doi.org/10.1061/(ASCE)HY.1943-7900.0001293.

Camenen, B., A. Bayram, and M. Larson. 2006. "Equivalent roughness height for plane bed under steady flow." *J. Hydraul. Eng.* 132 (11): 1146–1158. https://doi.org/10.1061/(ASCE)0733-9429(2006)132:11(1146).

Cellino, M., and W. H. Graf. 1999. "Sediment-laden flow in open-channels under noncapacity and capacity conditions." *J. Hydraul. Eng.* 125 (5): 455–462. https://doi.org/10.1061/(ASCE)0733-9429(1999)125:5(455).

Coleman, N. L. 1970. "Flume studies of the sediment translet coefficient." *Water Resour. Res.* 6 (3): 801–809. https://doi.org/10.1029/WR006i003p00801.

Coleman, N. L. 1981. "Velocity profiles with suspended sediment." *J. Hydraul. Res.* 22 (4): 263–289. https://doi.org/10.1080/00221688409499383.

Dey, S. 2014. *Fluvial hydrodynamics*. New York: Springer.

Einstein, H. A. 1955. *Effect of heavy sediment concentration near the bed on velocity and sediment distribution*. Berkeley, CA: Univ. California, Berkeley.

Finn, J. R., and M. Li. 2016. "Regimes of sediment-turbulence interaction and guidelines for simulating the multiphase bottom boundary layer." *Int. J. Multiphase Flow* 85 (Oct): 278–283. https://doi.org/10.1016/j.ijmultiphaseflow.2016.06.007.

Fromant, G., D. Hurther, J. Van der Zanden, A. D. A. Van Der, I. Cáceres, T. O'Donoghue, and J. S. Ribberink. 2019. "Wave boundary layer hydrodynamics and sheet flow properties under large-scale plunging-type breaking waves." *J. Geophys. Res. Oceans* 124 (1): 75–98. https://doi.org/10.1029/2018JC014406.

Fromant, G., R. S. Mieras, T. Revil-Baudard, J. A. Puleo, D. Hurther, and J. Chauchat. 2018. "On Bedload and suspended load measurement performances in sheet flows using acoustic and conductivity profilers." *J. Geophys. Res. Earth Surf.* 123 (10): 2546–2562. https://doi.org/10.1029/2017JF004560.

Garbini, J. L., F. K. Forster, and J. E. Jorgensen. 1982. "Measurement of fluid turbulence based on pulsed ultrasound techniques. Part 2. Experimental investigation." *J. Fluid Mech.* 118 (1): 471–505. https://doi.org/10.1017/S0022112082001165.

García, M. H. 2008. "Sediment transport and morphodynamics." In Vol. 110 of *ASCE manuals and reports on engineering practice*, 21–163. Reston, VA: ASCE.

Graf, W. H., and M. Cellino. 2002. "Suspension flows in open channels; experimental study." *J. Hydraul. Res.* 40 (4): 435–447. https://doi.org/10.1080/00221680209499886.

Guta, H., D. Hurther, and J. Chauchat. 2020. "Turbulent sediment transport processes in energetic sediment-laden open-channel flows." In *Proc., 10th Conf. on Fluvial Hydraulics*, 227–235. Delft, Netherlands: A.A. Balkema.

Hsu, T. J., J. T. Jenkins, and P. L. F. Liu. 2004. "On two-phase sediment transport: Sheet flow of massive particles." *Proc. Royal Soc. London. Ser. A: Math. Phys. Eng. Sci.* 460 (2048): 2223–2250. https://doi.org/10.1098/rspa.2003.1273.

Hurther, D., and U. Lemmin. 2001. "A correction method for turbulence measurements with a 3D acoustic doppler velocity profiler." *J. Atmos. Ocean. Technol.* 18 (3): 446–458. https://doi.org/10.1175/1520-0426(2001)018<0446:ACMFTM>2.0.CO;2.

Hurther, D., P. Thorne, M. Bricault, U. Lemmin, and J. Barnoud. 2011. "A multi-frequency acoustic concentration and velocity profiler (ACVP) for boundary layer measurements of fine-scale flow and sediment transport processes." *Coast. Eng.* 58 (7): 594–605. https://doi.org/10.1016/j.coastaleng.2011.01.006.

Kironoto, B., and W. H. Graf. 1994. "Turbulence characteristics in rough uniform open-channel." *Proc. Inst. Civ. Eng. Water, Marit. Energy* 106 (4): 333–344. https://doi.org/10.1680/iwtme.1994.27234.

Lyn, D. A. 1986. *Turbulence and turbulent transport in sediment-laden open-channel flows*. Rep. No. KH-R-49. Ann Arbor, MI: Univ. Microfilms International.

Lyn, D. A. 1988. "A similarity approach to turbulent sediment-laden flows in open channels." *J. Fluid Mech.* 193: 1–26. https://doi.org/10.1017/S0022112088002034.

Lyn, D. A. 2008. "Turbulence models for sediment transport engineering." In *Sedimentation engineering*, 763–825. Reston, VA: ASCE.

Muste, M., K. Yu, I. Fujita, and R. Ettema. 2005. "Two-phase versus mixed-flow perspective on suspended sediment transport in turbulent channel flows." *Water Resour. Res.* 41 (10): 1–22. https://doi.org/10.1029/2004WR003595.

Nezu, I., and H. Nakagawa. 1993. *Turbulence in open channel flows*. Rotterdam, Netherlands: A.A. Balkema.

Nezu, I., and W. Rodi. 1986. "Open-channel flow measurements with a laser doppler anemometer." *J. Hydraul. Eng.* 112 (5): 335–355. https://doi.org/10.1061/(ASCE)0733-9429(1986)112:5(335).

Nikora, V. I., and D. G. Goring. 2002. "Fluctuations of suspended sediment concentration and turbulent sediment fluxes in an open-channel flow." *J. Hydraul. Eng.* 128 (2): 214–224. https://doi.org/10.1061/(ASCE)0733-9429(2002)128:2(214).

Recking, A., P. Frey, A. Paquier, P. Belleudy, and J. Y. Champagne. 2008. "Feedback between bed load transport and flow resistance in gravel and cobble bed rivers." *Water Resour. Res.* 44 (5): 1–21. https://doi.org/10.1029/2007WR006219.

Revil-Baudard, T., J. Chauchat, D. Hurther, and P. Barraud. 2015. "Investigation of sheet-flow processes based on novel acoustic high-resolution velocity and concentration measurements." *J. Fluid Mech.* 767: 1–30. https://doi.org/10.1017/jfm.2015.23.

Revil-Baudard, T., J. Chauchat, D. Hurther, and O. Eiff. 2016. "Turbulence modifications induced by the bed mobility in intense sediment-laden flows." *J. Fluid Mech.* 808: 469–484. https://doi.org/10.1017/jfm.2016.671.

Ribberink, J. S., J. J. van der Werf, T. O'Donoghue, and W. N. M. Hassan. 2008. "Sand motion induced by oscillatory flows: Sheet flow and vortex ripples." *J. Turbul.* 9: 20. https://doi.org/10.1080/14685240802220009.

Rickenmann, D. 1991. "Hyperconcentrated flow and sediment transport at steep slopes." *J. Hydraul. Eng.* 117 (11): 1419–1439. https://doi.org/10.1061/(ASCE)0733-9429(1991)117:11(1419).

Rouse, H. 1938. "Experiments on the mechanics of sediment suspension." In *Proc., 5th Int. Congress of Applied Mech.*, 550–554. New York: Wiley.

Smith, J. D., and S. R. McLean. 1977. "Spatially averaged flow over a wavy surface." *J. Geophys. Res.* 82 (12): 1735–1746. https://doi.org/10.1029/JC082i012p01735.

Sumer, B. M., A. Kozakiewicz, J. Fredsøe, and R. Deigaard. 1996. "Velocity and concentration profiles in sheet-flow layer of movable bed." *J. Hydraul. Eng.* 122 (10): 549–558. https://doi.org/10.1061/(ASCE)0733-9429(1996)122:10(549).

Thorne, P. D., and D. Hurther. 2014. "An overview on the use of backscattered sound for measuring suspended particle size and concentration profiles in non-cohesive inorganic sediment transport studies." *Cont. Shelf Res.* 73 (Feb): 97–118. https://doi.org/10.1016/j.csr.2013.10.017.

van Rijn, L. 1984. "Sediment transport, Part II: : Suspended load transport." *J. Hydraul. Eng.* 110 (11): 1613–1641. https://doi.org/10.1061/(ASCE)0733-9429(1984)110:11(1613).

Wilson, K. 1987. "Analysis of bed-load motion at high shear stress." *J. Hydraul. Eng.* 113 (1): 97–103. https://doi.org/10.1061/(ASCE)0733-9429(1987)113:1(97).

Wilson, K. 1989. "Mobile-bed friction at high shear stress." *J. Hydraul. Eng.* 115 (6): 825–830. https://doi.org/10.1061/(ASCE)0733-9429(1989)115:6(825).